ACS APPLIED MATERIALS & INTERFACES

Research Article

www.acsami.org

High Performance Solid-State Electric Double Layer Capacitor from Redox Mediated Gel Polymer Electrolyte and Renewable Tamarind Fruit Shell Derived Porous Carbon

S. T. Senthilkumar,[†] R. Kalai Selvan,*[,†] J. S. Melo,[‡] and C. Sanjeeviraja[§]

[†]Solid State Ionics and Energy Devices Laboratory, Department of Physics, Bharathiar University, Coimbatore-641046, Tamil Nadu, India

[‡]Nuclear Agriculture and Biotechnology Division, Bhabha Atomic Research Centre, Trombay, Mumbai-400085, India

[§]Department of Physics, Alagappa Chettiar College of Engineering, Karaikudi, 630 004, Tamil Nadu, India

Supporting Information

ABSTRACT: The activated carbon was derived from tamarind fruit shell and utilized as electrodes in a solid state electrochemical double layer capacitor (SSEDLC). The fabricated SSEDLC with PVA (polyvinyl alcohol)/H_2SO_4 gel electrolyte delivered high specific capacitance and energy density of 412 F g^{-1} and 9.166 W h kg^{-1}, respectively, at 1.56 A g^{-1}. Subsequently, Na_2MoO_4 (sodium molybdate) added PVA/H_2SO_4 gel electrolyte was also prepared and applied for SSEDLC, to improve the performance. Surprisingly, 57.2% of specific capacitance (648 F g^{-1}) and of energy density (14.4 Wh kg^{-1}) was increased while introducing Na_2MoO_4 as the redox mediator in PVA/H_2SO_4 gel electrolyte. This improved performance is owed to the redox reaction between Mo(VI)/Mo(V) and Mo(VI)/Mo(IV) redox couples in Na_2MoO_4/PVA/H_2SO_4 gel electrolyte. Similarly, the fabricated device shows the excellent capacitance retention of 93% for over 3000 cycles. The present work suggests that the Na_2MoO_4 added PVA/H_2SO_4 gel is a potential electrolyte to improve the performance instead of pristine PVA/H_2SO_4 gel electrolyte. Based on the overall performance, it is strongly believed that the combination of tamarind fruit shell derived activated carbon and Na_2MoO_4/PVA/H_2SO_4 gel electrolyte is more attractive in the near future for high performance SSEDLCs.

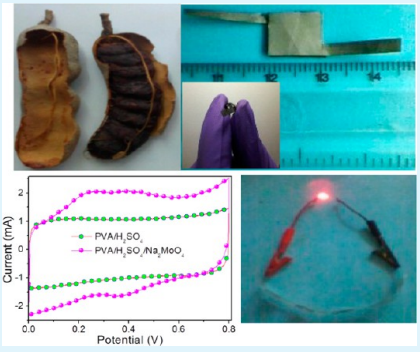

KEYWORDS: *tamarind fruit shell, activated carbon, redox additive, specific capacitance, electric double layer capacitor*

1. INTRODUCTION

Electrochemical double layer capacitors (EDLCs), also known as electrochemical capacitors (ECs), have recently played a vital role in the area of charge storage devices and are used for various potential applications owing to their high power, acceptable energy density, and long cycle with high safety.[1,2] However, their wide applications are commonly diminished by certain problems such as electrolyte leakage, corrosion, and packing since commercially available EDLCs are fabricated by using liquid electrolytes.[3,4] Moreover, the liquid electrolytes release some hazardous byproduct into the environment.[4] These issues can be skirted by utilizing polymer based electrolytes in EDLCs which are known as solid state EDLCs. However, the SSEDLCs deliver low capacitance and energy density compared to liquid electrolytes.[5] In order to overcome these drawbacks, recently researchers are identifying some new innovative approaches.

It is well known that the activated carbons (ACs) are mostly used electrode material in commercial EDLCs because of their high surface area, good electrochemical stability, electrical conductive properties, micro- (<2 nm) to mesoporous (2−50 nm) nature, and so forth.[6] However, the large scale production of EDLCs is hindered by increasing raw materials cost and less availability of precursors. However, the applications of AC are increasing day by day. Hence, conventional raw materials like fossil fuels of petroleum coke, tar pitches, and coal[7] do not meet out our demand of large scale production of AC because of their less availability and because they are not renewable in nature. Recently, these requirements are immensely fulfilled by utilization of bio-waste as precursor for AC preparation because of low cost, accessibility, and being naturally renewable as well as waste management.[6] Also, there are some reports available for preparation of AC from various bio-wastes for EDLC applications. For example, neem leaves derived AC provided the maximum capacitance of 400 F g^{-1} at 0.5 A g^{-1} in 1 M H_2SO_4 and 88 F g^{-1} at 2 A g^{-1} in 1 M $LiPF_6$ in EC/DEC (ethylene carbonate/diethyl carbonate) electrolytes.[8] The AC prepared from celtuce leaves delivered the best capacitance values of 273 F g^{-1} at 0.5 A g^{-1} in 2 M KOH.[9] Similarly, coconut shell and corn grain based ACs were also utilized as effective electrode materials and achieved the specific capacitance of 228 and 257 F g^{-1}, respectively.[10,11] From that, it can be understood that the performance of the AC varies for different bio-waste based on

Received: June 5, 2013
Accepted: September 30, 2013
Published: October 28, 2013

 © 2013 American Chemical Society

their nature. Moreover, calcium-rich carbon material was prepared from tamarind (*Tamarindus indica*) fruit shells for water purification[12] but the capacitance performance of the AC derived from tamarind fruit shells is not reported so far. Tamarind is a tree which is grown worldwide (especially in tropical and subtropical countries such as Africa, India, China, etc.), and it is mainly cultivated for its sour fruit pulp. Tamarind fruit pulp is covered by an outer shell (Figure 1) which is commonly considered as waste material because it is a byproduct of tamarind fruit pulp.

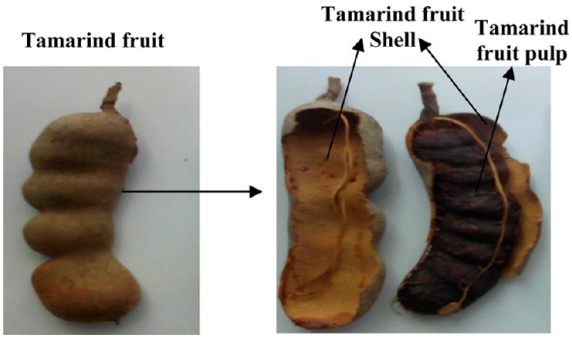

Figure 1. Images of tamarind fruit and its major parts.

Recently, the literature depicts that the introduction of redox additives or mediators or compounds such as *p*-phenylenediamine,[13] *m*-phenylenediamine,[14] indigo carmine,[15] hydroquinone,[16] KI,[6] and $VOSO_4$[17] into the liquid electrolytes immensely enhanced the total specific capacitance and energy density of the EDLCs through their electron transfer redox reactions. However, this type of strategy using redox additives in gel polymer electrolytes is not well explored so far, and hence, this kind of versatile approach opened up a new avenue to identify the novel redox additives. The following properties are very important to use the species as redox additives in that it should involve in redox reaction, better solubility, electrochemically stable, easy preparation, and nontoxic. Ours is the first report for fabricating SSEDLCs using tamarind fruit shell derived AC as the efficient electrode and Na_2MoO_4 (redox additive) mediated PVA/H_2SO_4 as polymer electrolyte. This newly identified Na_2MoO_4 mediated polymer electrolyte enhances the performance, since the MoO_4^{2-} species can easily be converted into a polymeric ion of H_2MoO_4 (i.e., monomeric species) in acidic medium, which is actively involved in redox reaction.[18−20] As expected, the Na_2MoO_4 mediated polymer (PVA/H_2SO_4) electrolyte enhances nearly 57.2% of specific capacitance and energy density of the pristine PVA/H_2SO_4 polymer electrolyte. In detail, we have obtained 412 F g^{-1}; 9.16 Wh kg^{-1} for pristine PVA/H_2SO_4 polymer electrolyte and 648 F g^{-1}; 14.4 Wh kg^{-1} for $Na_2MoO_4/PVA/H_2SO_4$ polymer electrolyte. This attempt emphasizes the simple and safe preparation method with cost effectiveness for achieving better performance of the end device.

2. EXPERIMENTAL SECTION

2.1. Preparation and Characterization of AC. The activated carbons (ACs) were prepared from tamarind fruit shell as follows. The pulverized tamarind fruit shell was preheated at 200 °C for 24 h. Then the desired amount of preheated sample was activated in 20% (T20), 30% (T30), and 40% (T40) of KOH for 24 h, individually. Subsequently, they were carbonized at 700 °C for 4 h in Ar atmosphere individually. Then, the carbonized samples were washed with distilled water and a desired amount of 1 M HCl until the pH became ∼7 and finally dried at 100 °C overnight. Then, the BET surface area and pore size analysis of AC were done using an ASAP 2020 instrument. The microscopic porous structure of the AC was observed via scanning electron microscopy (SEM) (Quanta 200 ESEM, FEI), and the nanoporous structure of the AC was observed through high-resolution transmission electron microscopy (TEM; JEOL 2100F at 200 kV). Additionally, the physical and chemical properties of the AC were characterized by powder X-ray diffraction spectroscopy (XRD; X'Pert PRO X-ray DiffractometerPANalytical), Raman spectroscopy (Jobin-Yvon ISA T 64000), Fourier transform infrared spectroscopy (FT-IR; Bruker tensor 27), and X-ray photoelectron spectroscopy (XPS; Perkin-Elmer PHI-5702).

2.2. Gel Electrolyte Preparation. The PVA/H_2SO_4 polymer electrolyte and redox mediated PVA/H_2SO_4 polymer electrolyte were prepared in the following manner. First, 1 g of PVA (HiMedia, MW = 70 000−100 000) was mixed with 20 mL of hot (70 °C) water with constant stirring for 2 h to form a clear solution. Then, 1 g of diluted (10 ml, dis. H_2O) H_2SO_4 was added. Subsequently, after 1 h, 0.2 g of diluted (5 ml, dis. H_2O) Na_2MoO_4 was added to the above solution with constant stirring, and it was kept until formation of a gel-like solution.

2.3. Electrode Preparation and SSEDLCs Fabrication. The electrodes for SSEDLCs were prepared by drop casting method.[21] Initially, the slurry was prepared by mixing of AC (16 mg, 80%), carbon black (2 mg, 10%) (Sigma Aldrich), and polyvinylidene fluoride (2 mg, 10%) (Sigma-Aldrich, MW = 534 000) in 0.4 mL of *N*-methyl-2-pyrrolidone. Further, 12 μL of this slurry was spread onto the stainless steel (thickness = 0.04 mm) with an area of 1 cm^2 and dried at 50 °C for overnight. Based on the previous report,[21] the active material loading was (i.e., excluding carbon black and polyvinylidene fluoride) to be 0.48 mg on each electrode. The fabrication details of SSEDLCs were reported elsewhere.[22,23] The prepared gel electrolyte was coated on the surface of the electrodes and assembled together by face-to-face. Finally, the solid state capacitors were prepared by the evaporation of water at 40 °C for 6 h, besides being kept at room temperature for few (∼5 h) hours (i.e., where the polymer electrolyte was half-dried). The fabricated device and its schematic diagram are given in Figure 2a and b,

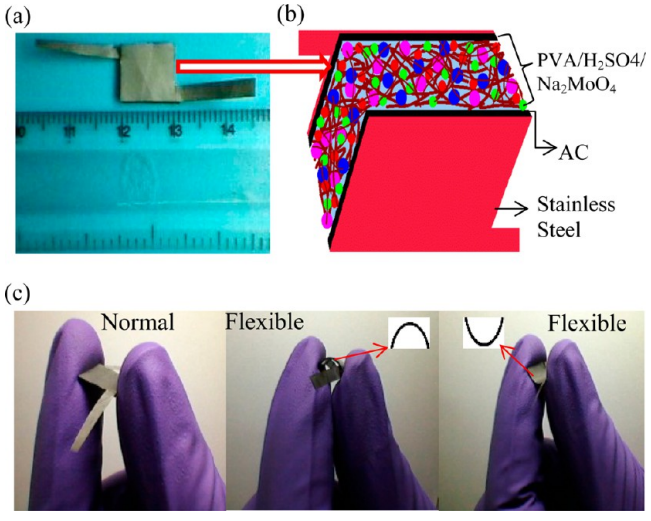

Figure 2. (a) Fabricated SSEDLCs and (b) schematic diagram of redox mediated polymer gel electrolyte used SSEDLCs. (c) Fabricated SSEDLC at normal and flexible state.

respectively. Also, the flexible behavior of SSEDLC is seen in Figure 2c. Moreover, for comparison studies, the PVA/KOH gel electrolyte and liquid electrolyte (H_2SO_4) used EDLCs were fabricated.

2.4. Electrochemical Studies of AC Electrodes and SSEDLCs. The electrochemical properties of the AC electrodes were studied by cyclic voltammetry (CV) and galvanostatic charge−discharge (GCD) using a three electrode system using activated carbon electrode as working electrode, Ag/AgCl/sat.KCl electrode as reference electrode,

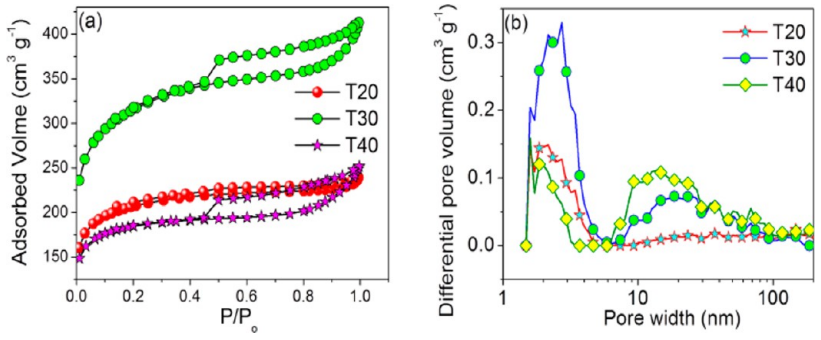

Figure 3. (a) N_2 adsorption−desorption isotherm. (b) Pore size distribution of ACs (T20, T30, and T40).

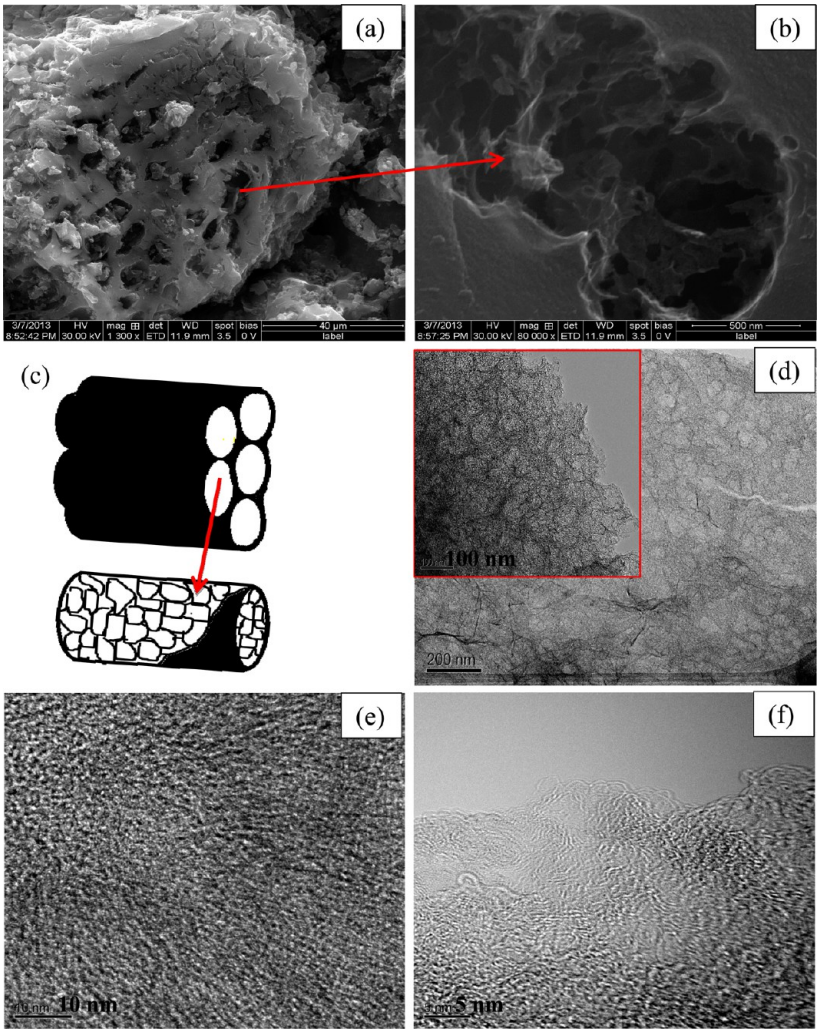

Figure 4. (a, b) Typical SEM image of AC (T30) and it is closer view of a single pore. (c) Schematic of pore structure image of AC (T30). (d−f) TEM and HRTEM images of AC (T30).

and Pt (purity of 99.99%) wire as counter electrode in 1 M H_2SO_4 solution at potential range from 0 to 0.8 V. Moreover, the electrochemical properties of the SSEDLCs were studied through CV for potential of 0−0.8 V at different scan rates from 10 to 200 mV s^{-1} and GCD test for potential of 0−0.8 V at different current densities from 1.56 to 10.4 A g^{-1}. Electrochemical impedance spectroscopy (EIS) was carried out at open circuit potential (OCP) by applying ac potential with 10 mV amplitude in the frequency ranges from 300 mHz to 1 MHz. Moreover, cycle life was tested at current density of 7.29 A g^{-1} for 3000 cycles. All the above electrochemical studies were carried out at room temperature using a Bio-Logic SP150 electrochemical workstation.

The specific capacitance of the AC electrodes was calculated by using the equation:[6]

$$C = \frac{I\Delta t}{m\Delta V} \quad (1)$$

where I is the applied current, m is the mass of the active material (AC) on electrode, Δt is the discharge time, and ΔV is the potential range after IR drop.

The specific capacitance of the cell (C_{cell}) and specific capacitance of the electrode (C_{SP}) were calculated using the following equations:[24]

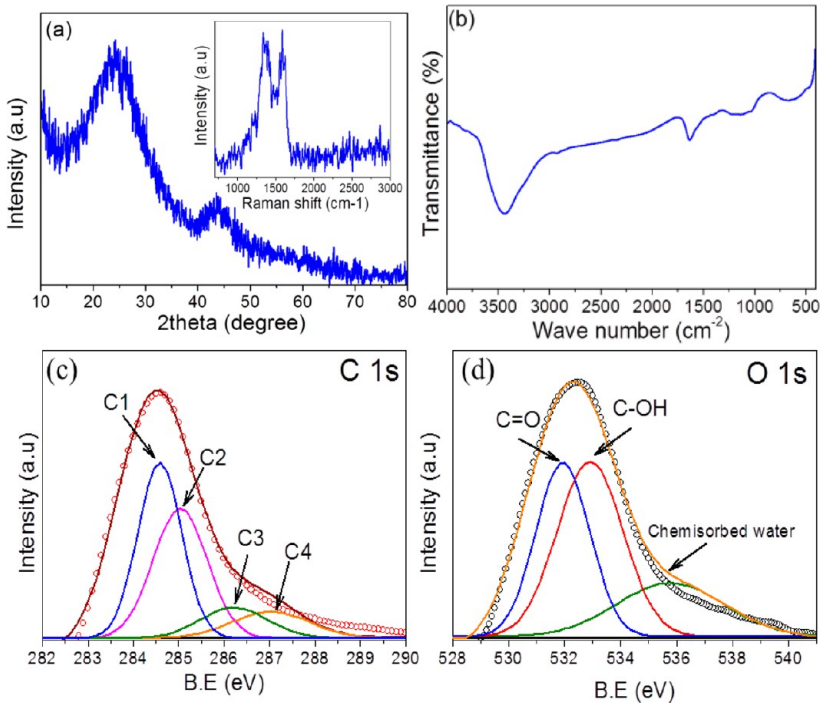

Figure 5. Typical (a) XRD pattern (inset: Raman spectrum), (b) FTIR spectrum, and (c,d) C 1s and O 1s XPS spectra of AC (T30).

$$C_{cell} = \frac{I\Delta t}{M\Delta V} \quad \text{and} \quad C_{SP} = 4C_{cell} \tag{2}$$

where M is the total mass of the active material in both electrodes.

Similarly, the energy (E_{cell}) and power (P_{cell}) density were calculated using the following equations:[24]

$$E_{cell} = \frac{C_{cell}\Delta V^2}{7.2}; \quad P_{cell} = \frac{E_{cell}}{\Delta t} \tag{3}$$

The average discharge current (I_d) from cyclic voltammogram, areal capacitance (C_a), and mean areal capacitance (C_m) were obtained using the following relations:[1,25]

$$I_d = \frac{\int Id\nu}{2\Delta V}; \quad C_a = \frac{I_d}{sA}; \quad C_m = \frac{\Delta I}{2\Delta sA} \tag{4}$$

where $\int Id\nu$ is the integral area of CV curve, ΔV is the potential difference, s is the scan rate, A is the area of active material in electrolyte, and $\Delta I/\Delta s$ is the slope value.

3. RESULTS AND DISCUSSION

3.1. Characterization of AC. The typical nitrogen (N_2) adsorption−desorption isotherm and pore size distribution of the prepared AC (T20, T30 and T40) are shown in Figure 3. Here, all the ACs display the type IV adsorption−desorption isotherm, and the observed hysteresis loop between the adsorption−desorption branch (Figure 3a) describes the presence of mesopores (2−50 nm). Further, the low pressure ($P/P_0 < 0.5$) hysteresis indicates the existence of micropores (<2 nm).[26] The BET surface area of ACs such as T20, T30, and T40 are 673.43, 1040.31, and 593.82 $m^2\ g^{-1}$, respectively. Among these, T30 shows the higher surface area (1040.31 $m^2\ g^{-1}$). Similarly, the high pore volume value of 0.61 $cm^3\ g^{-1}$ was obtained for T30, while it is 0.36 $cm^3\ g^{-1}$ for T20 and 0.37 $cm^3\ g^{-1}$ for T40.

Moreover, the pore size distribution curves (Figure 3b) indicate that the ACs have well developed mesopores and few micropores. The micro-mesopore and mesopore distributions of the ACs are in the range of ∼1.4−4 nm and ∼7−50 nm. Furthermore, Figure 4a displays the typical SEM image of T30 which shows the porous morphology with bundlelike pore structure. Figure 4b shows the closer view of the single pore which indicates the presence of graphene-like nanosheets inside of the pore, and a schematic of pore structure is shown in Figure 4c. Besides, the TEM image (Figure 4d and its inset) shows the existence of porous morphology of AC (T30). Additionally, the observed pore size of ∼3 nm infers the mesoporous nature, and further the formation of amorphous graphitic carbon was revealed from Figure 4e and f of AC (T30).

The representative XRD, Raman, FT-IR, and XPS pattern of T30 is given are Figure 5. The XRD pattern shows two broad peaks (Figure 5a) at 2θ of about 23° and 43° corresponding to the (002) and (100) plane reflection and reveals the amorphous nature of activated carbon.[27,28] The Raman spectra (Figure 5a (inset)) also substantiate the highly disordered carbon structure. The peak at about ∼1352 cm^{-1} corresponds to the D band which indicates the breathing mode vibration of A_{1g}, related to disordered carbon. The observed G band at ∼1561 cm^{-1} corresponds to in-plane stretching vibration mode of E_{2g} in sp^2 carbons.[29,30] The peak at 3442 cm^{-1} in FT-IR spectra (Figure 5b) is attributed to the hydroxyl group and chemisorbed water. A small sharp peak at 1633 cm^{-1} is ascribed to the C═O group.[31] Moreover, the broad peak centered at 1122 cm^{-1} corresponds to the C−O group. Another broad peak centered at 667 cm^{-1} is a characteristic of the out-of-plane deformation of C−H groups in different substituted benzene rings.[32,33] Further, the XPS measurement was also carried out to identify the presence of surface functional groups on AC and its survey spectra is shown in Figure S2 in the Supporting Information. Besides, the resolved C 1s and O 1s peaks of AC were identified in this spectra, and its corresponding core-level spectra are given in Figure 5c and d. The C 1s spectrum holds the four peaks such as 284.6 (C1), 285.1 (C2), 286.2 (C3), and 287.1 (C4) eV that are attributed to the graphitic (C−C)/C−H groups, hydroxyl groups (C−OH),

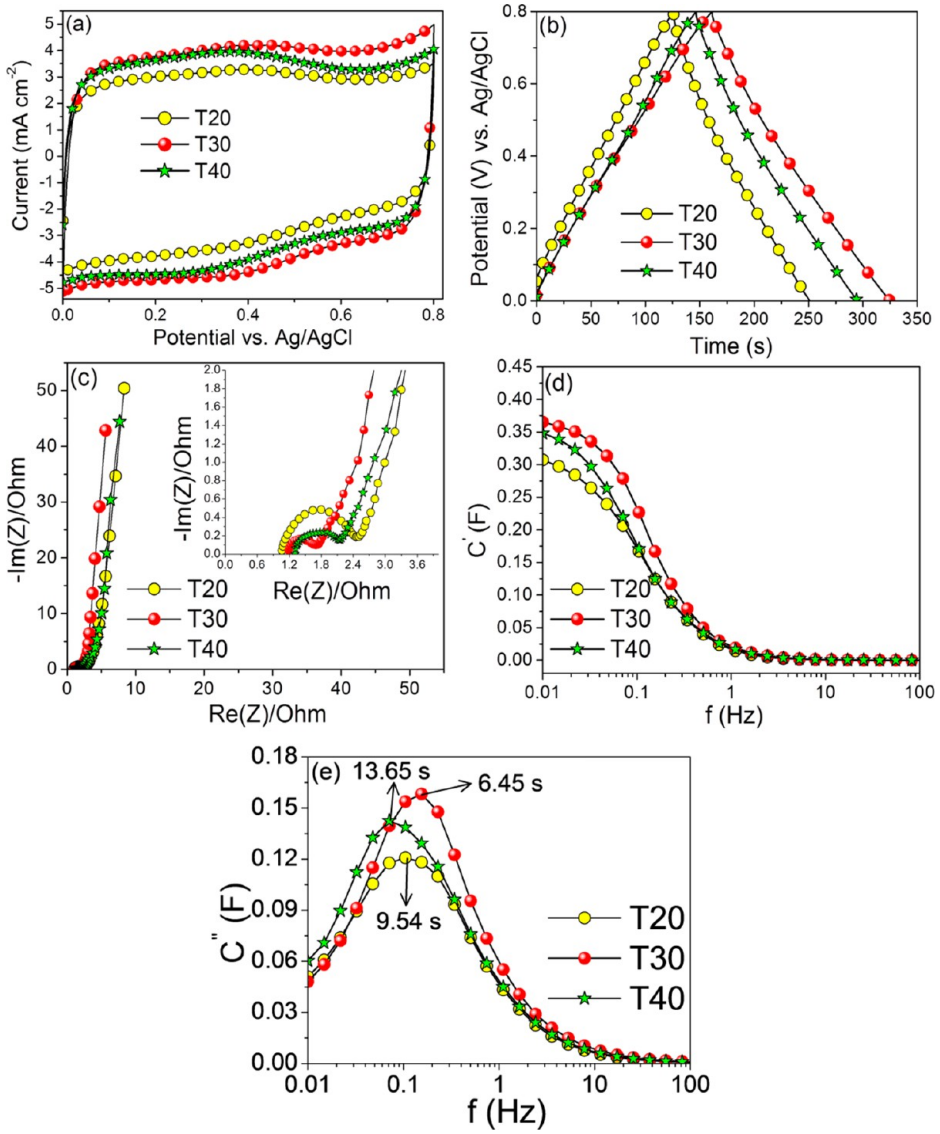

Figure 6. (a) CV at scan rate of 10 mV s^{-1}, (b) GCD curves at 2.1 A g^{-1} of AC electrodes (T20, T30 and T40), (c) Nyquist plots of AC electrodes, (d) C′ vs frequency, and (e) C″ vs frequency.

Table 1. Surface Area, Pore Volume, Pore Size, and Capacitance of the Prepared Activated Carbons

sample	BET surface area (m^2 g^{-1})	pore volume (cm^3 g^{-1})[a]	pore diameter (nm)[a]	microporous surface area (m^2 g^{-1})[b]	micropore volume (cm^3 g^{-1})[b]	max C_{sp} at 2.1 mA cm^{-2} (F g^{-1})[c]
T20	673.43	0.36	2.13	436.3	0.22	325.5
T30	1040.31	0.61	2.35	586.8	0.29	425.8
T40	593.82	0.37	2.49	414.47	0.20	394

[a]Total pore volume calculated at P/P_0 = 0.99 and average pore diameter from BET method. [b]Microporous surface area and micropore volume from *t*-plot method. [c]Specific capacitance calculated from single electrode system.

phenol/ether (C−O) groups, and carbonyl/quinone groups (C═O), respectively. Moreover, the three peaks are noted at 531.8, 532, and 535.8 eV in O 1s core level spectra which originate from carbonyl/quinone groups (C═O), hydroxyl groups (C−OH), and chemisorbed water.[34−36]

3.2. Electrochemical Characterization of AC Electrodes. The electrochemical properties of the AC electrodes were tested using CV and GCD by three electrode systems, and the obtained results are shown in Figure 6. The quasi-rectangular CV curves are acquired for all the ACs (Figure 6a), which indicates the presence of pseudocapacitance due to the occurrence of reversible redox reaction. This usually happens between the oxygen functionalities like carbonyl (C═O), hydroxyl (C−OH), and H^+.[37,38] However, among ACs, T30 covers the high current area which indicates the storage of higher capacitance than T20 and T40. Likewise, T30 exhibits the high areal capacitance of 197 mF cm^{-2} at 10 mV s^{-1} but it is 150 mF cm^{-2} for T20 and 181 mF cm^{-2} for T40. A substantial high specific capacitance of 425.8 F g^{-1} was obtained for T30 from the charge−discharge curve (Figure 6b) at 2.1 A g^{-1}, while the obtained specific capacitances for T20 and T40 are 325.5 and 394 F g^{-1}, respectively. Here, this high specific capacitance performance of T30 could be owed to their

dx.doi.org/10.1021/am402162b | ACS Appl. Mater. Interfaces 2013, 5, 10541−10550

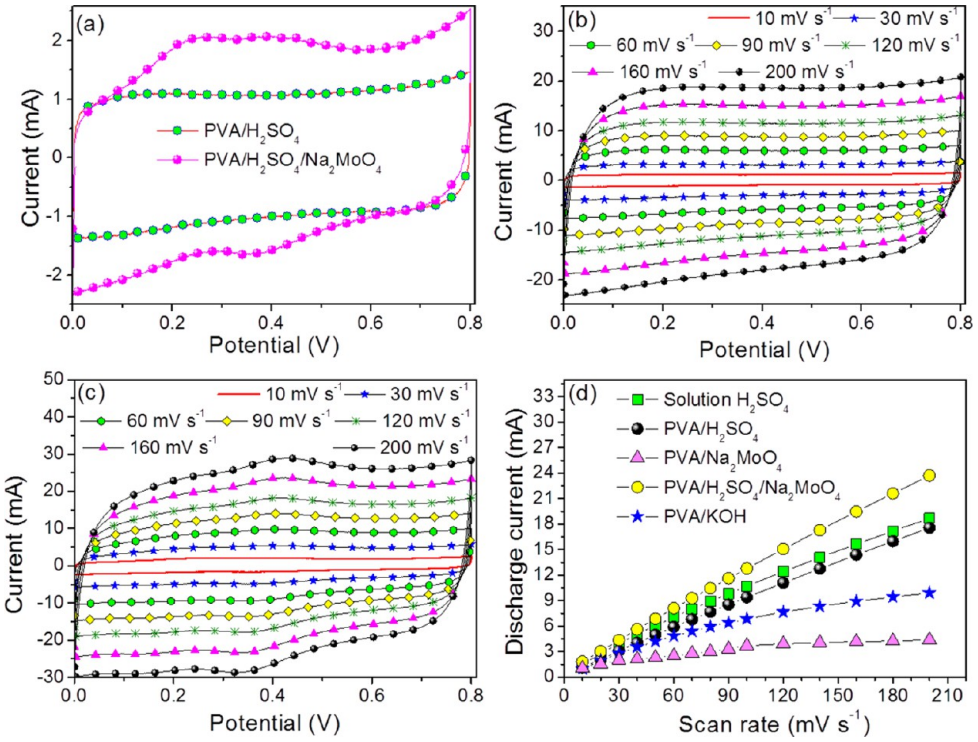

Figure 7. (a) CV curves of PVA/H_2SO_4 and $PVA/H_2SO_4/Na_2MoO_4$ gel electrolyte used cells at 10 mV s^{-1}. (b, c) CV curves of PVA/H_2SO_4 and $PVA/H_2SO_4/Na_2MoO_4$ gel electrolyte used SSEDLCs at different scan rate. (d) Discharge current of solution H_2SO_4, PVA/H_2SO_4, PVA/Na_2MoO_4, $PVA/H_2SO_4/Na_2MoO_4$, and PVA/KOH electrolyte used SSEDLCs as a function of scan rate.

high surface area and pore volume (1040.31 m^2 g^{-1} and 0.61 cm^3 g^{-1}) among the ACs (for detail, see Table 1).

Furthermore, the solution resistance and charge transfer resistance of the AC electrodes were also calculated from Nyquist plot (Figure 6c). The calculated solution resistance and charge transfer resistance of T20, T30, and T40 are 1.05, 1.18 Ω; 1.3, 1.42 Ω; and 0.6, 0.83 Ω, respectively. Nonetheless, T30 has a low solution resistance and charge transfer resistance. The real and imaginary parts of capacitance (C' and C'') of the electrodes with respect to frequency are shown in Figure 6c, d. The order of the real part capacitance of the electrodes is T30 (0.36 F) > T40 (0.34 F) > T20 (0.31 F) where T30 shows the better capacitance, and this behaviour coincides with the results of CV and charge–discharge. The calculated relaxation time[39] ($\tau_0 = 1/f_0$) of T20, T30, and T40 are (Figure 6e) 9.54, 6.45, and 13.65 s, respectively. However, T30 exhibits the low relaxation time (τ_0) which indicates fast frequency response as well as its better charge storage and delivery behavior. Overall, based on the above results, T30 exhibits the good electrochemical performance among the AC electrodes. In this regard, T30 is considered as a superior and optimal AC electrode for the fabrication of EDLC.

3.3. Electrochemical Characterization of SSEDLCs. Figure 7a shows the CV of fabricated SSEDLCs using PVA/H_2SO_4 and $PVA/H_2SO_4/Na_2MoO_4$ gel electrolyte at 10 mV s^{-1}. Almost rectangular behavior was observed for PVA/H_2SO_4 that infers the capacitance is stored by an accumulation of electrolyte ions between the electrode/electrolyte interfaces which is known as electric double layer capacitance. Moreover, it maintains the rectangular behavior even at high scan rate up to 200 mV s^{-1} (Figure 7b) which indicates the high rate electrochemical performance.[6,40] On the other hand, while using $PVA/H_2SO_4/Na_2MoO_4$ as gel electrolyte, it shows a redox peak. It indicates the presence of pseudo-capacitance nature, which is due to the redox between the possible redox couples Mo(VI)/Mo(V) and Mo(VI)/Mo(IV) [$Mo(VI) + e^- \leftrightarrow Mo(V)$ and $Mo(VI) + 2e^- \leftrightarrow Mo(IV)$]. In detail, the molybdate species (MoO_4^{2-}) has the tendency to form a polymeric ion (H_2MoO_4) in acidic medium[18−20] (where the oxidation state is +VI) and thus polymeric ions (H_2MoO_4) can be involved in redox reactions. Therefore the possible redox reactions may be as follows.[18−20]

During forward scan,

$$H_2Mo(VI)O_4 + 2e^- + 2H^+ \rightarrow H_2Mo(IV)O_3 + H_2O \quad (5)$$

$$H_2Mo(VI)O_4 + e^- + H^+ \rightarrow HMo(V)O_3 + H_2O \quad (6)$$

During backward scan,

$$H_2Mo(IV)O_3 \rightarrow HMo(V)O_3 + e^- + H^+ \rightarrow Mo(VI)O_3 + e^- + H^+ \quad (7)$$

$$HMo(V)O_3 \rightarrow Mo(VI)O_3 + e^- + H^+ \quad (8)$$

$$Mo(VI)O_3 + H_2O \rightarrow Mo(VI)O_4^{2-} + 2H^+ \rightarrow H_2Mo(VI)O_4 \quad (9)$$

Nonetheless, PVA/Na_2MoO_4 gel electrolyte displays (Figure S4a, Supporting Information) a rectangular CV curve as reported elsewhere,[41] wherein the molybdate (MoO_4^{2-}) ions are electrochemically inactive in its own (Na_2MoO_4) medium. Hence, this result substantiates that the redox reactions of the molybdate occurred in acidic medium by the form of polymeric ions (H_2MoO_4).[18−20] Besides, $PVA/H_2SO_4/Na_2MoO_4$ gel electrolyte covers the large current area in the CV curve which reveals

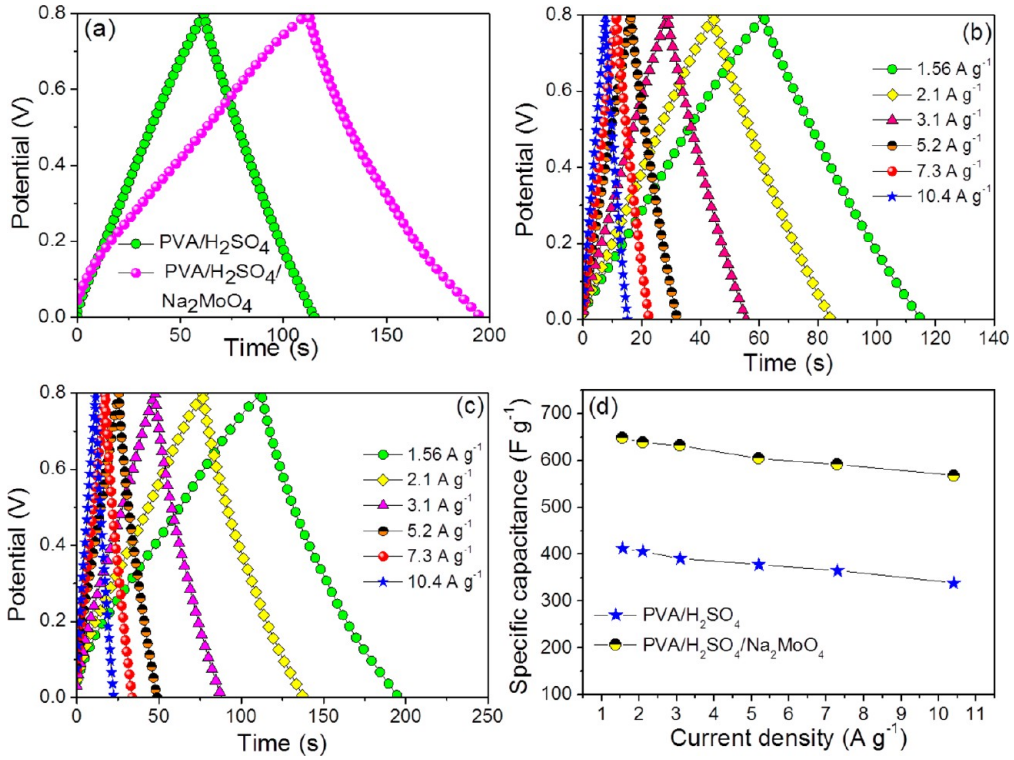

Figure 8. (a) Comparison of GCD curves at 1.56 A g^{-1}. (b, c) GCD curves of PVA/H_2SO_4 and $PVA/H_2SO_4/Na_2MoO_4$ gel electrolyte used SSEDLCs at 1.56−10.4 A g^{-1}. (d) Specific capacitance of SSEDLCs as a function of current density.

their improved capacitance performance through their possible redox reactions of polymeric ions (H_2MoO_4) in $PVA/H_2SO_4/Na_2MoO_4$ gel electrolyte. Moreover, it also shows high rate electrochemical performance unlike PVA/H_2SO_4 and PVA/Na_2MoO_4 gel electrolytes (see Figure S4b in the Supporting Information) because the reversible redox peaks are clearly present even at high scan rate (200 mV s^{-1}) (Figure 7c).

The relation between discharge current and scan rate (from 10 to 200 mV s^{-1}) at 0.8 V of PVA/H_2SO_4, PVA/Na_2MoO_4 and $PVA/H_2SO_4/Na_2MoO_4$ gel electrolyte are given in Figure 7d. For comparison we have also given the discharge current behavior with scan rate of liquid (H_2SO_4) electrolyte and PVA/KOH gel electrolyte used EDLCs (the corresponding CV curves are given in Figure S3 in the Supporting Information). The excellent linear discharge current behavior is noted for $PVA/H_2SO_4/Na_2MoO_4$ gel electrolyte compared to pristine PVA/H_2SO_4, PVA/KOH and H_2SO_4 liquid electrolyte. However, the more deviated linear discharge current behavior is noted at increasing scan rate for PVA/Na_2MoO_4 and PVA/KOH gel electrolyte. Here, the linear and nonlinear discharge current behaviors indicate the better and narrow electrolyte ion diffusion into the bulk electrode. Moreover, the mean areal capacitance was calculated from Figure 7d. The maximum mean areal capacitance of 55 mF cm^{-2} was obtained for $PVA/H_2SO_4/Na_2MoO_4$ gel electrolyte than pristine PVA/H_2SO_4 (43 mF cm^{-2}), PVA/Na_2MoO_4 (10 mF cm^{-2}), PVA/KOH (22.5 mF cm^{-2}), and H_2SO_4 liquid electrolyte (44 mF cm^{-2}), and also it is higher than the earlier reports.[1] Interestingly, after addition of Na_2MoO_4 into the PVA/H_2SO_4 gel electrolyte, 21.8% of mean areal capacitance was increased when compared with pristine PVA/H_2SO_4 gel electrolyte. Here, the PVA/Na_2MoO_4 gel electrolyte exhibits lower mean areal capacitance than other electrolytes.

Subsequently, the areal capacitance was calculated from CV at 10 mV s^{-1} corresponding to 115, 85, 78, 129, and 81 mF cm^{-2} for solutions H_2SO_4, PVA/H_2SO_4, PVA/Na_2MoO_4, $PVA/H_2SO_4/Na_2MoO_4$, and PVA/KOH, respectively. Interestingly, $PVA/H_2SO_4/Na_2MoO_4$ gel electrolyte shows 52% improved areal capacitance compared to pristine PVA/H_2SO_4 gel electrolyte due to their redox reactions between the redox couples of Mo(VI)/Mo(V) and Mo(VI)/Mo(IV). Besides, PVA/H_2SO_4 gel electrolyte shows a 35.3% lower areal capacitance than liquid electrolyte, and this is mostly due to the poor electrolyte−electrode contact area, low ionic mobility, and ion accessibility with electrode compared to liquid electrolytes. However, after introduction of Na_2MoO_4 into PVA/H_2SO_4 gel electrolyte, it exhibits a 12.1% higher areal capacitance than the liquid electrolyte, through the redox reactions of (Mo(VI)/Mo(V) and Mo(VI)/Mo(IV)). So the introduction of redox additives into the polymer electrolyte can improve the performance even higher than liquid electrolyte.

The capacitance performance of SSEDLCs using PVA/H_2SO_4 and $PVA/H_2SO_4/Na_2MoO_4$ gel electrolyte were examined through GCD test (Figure 8a−c). Also, for comparison, the GCD curve of the PVA/Na_2MoO_4 gel electrolyte is also given in Figure S4c in the Supporting Information. The triangle and deviated triangle behavior was observed for PVA/H_2SO_4 and $PVA/H_2SO_4/Na_2MoO_4$ gel electrolyte, respectively, which elucidates the ideal (or electric double layer (EDL)) and nonideal (or redox) capacitive behavior. Figure 8d describes the performance of specific capacitance with respect to current density. The high specific capacitance and energy density of 648 F g^{-1} at 1.56 A g^{-1} and 14.4 W h kg^{-1} at 625 W kg^{-1} (see Figure 9) were achieved for $PVA/H_2SO_4/Na_2MoO_4$ gel electrolyte, while that of PVA/H_2SO_4 and PVA/Na_2MoO_4 gel electrolytes delivered only 412 F g^{-1}, 9.16 W h kg^{-1} and 364 F g^{-1}, 8 W h

dx.doi.org/10.1021/am402162b | ACS Appl. Mater. Interfaces 2013, 5, 10541−10550

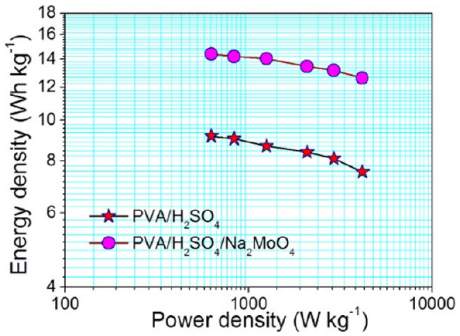

Figure 9. Ragone plots of PVA/H_2SO_4 and PVA/H_2SO_4/Na_2MoO_4 gel electrolyte used SSEDLCs.

kg^{-1} (see Figure S4d, Supporting Information). Such results show 57.2% and 78% improved performance over pristine PVA/H_2SO_4 and PVA/Na_2MoO_4 gel electrolyte. Here, this improved capacitance/energy performance is because of the possible redox reactions (see eqs 5−9) of polymeric ions (H_2MoO_4) in PVA/H_2SO_4/Na_2MoO_4 gel electrolyte. Moreover, the obtained energy density is higher than that of previously reported solid state hybrid capacitors such as polypyrrole/phosphomolybdic acid//poly(3, 4-ethylenedioxythiophene)/phosphothugstic acid, 4 Wh kg^{-1};[42] redox/hybrid materials used solid state supercapacitor ((poly(3,4-ethynendioxythiophene)//(poly(3,4-ethynendioxythiophene)), 4.25 Wh kg^{-1}; carbon nanoparticle/MnO_2//carbon nanoparticle/MnO_2, 4.8 Wh kg^{-1}; RuO_2/carbon//RuO_2/carbon, 10 Wh kg^{-1}, and polypyrrole//polypyrrole.[43−46]

The electrochemical conductive and kinetic properties of PVA/H_2SO_4 and PVA/H_2SO_4/Na_2MoO_4 gel electrolyte were tested using EIS at open circuit potential in the frequency range from 300 mHz to 1 MHz. The corresponding Nyquist plots are shown in Figure 10a. It can be seen that both systems exhibit semicircles at high frequency which explains the internal (charge transfer) resistance of the SSEDLCs.[47] The large semicircle observed for PVA/H_2SO_4/Na_2MoO_4 gel electrolyte infers the larger ionic resistance,[47] and it is due to the addition of Na_2MoO_4

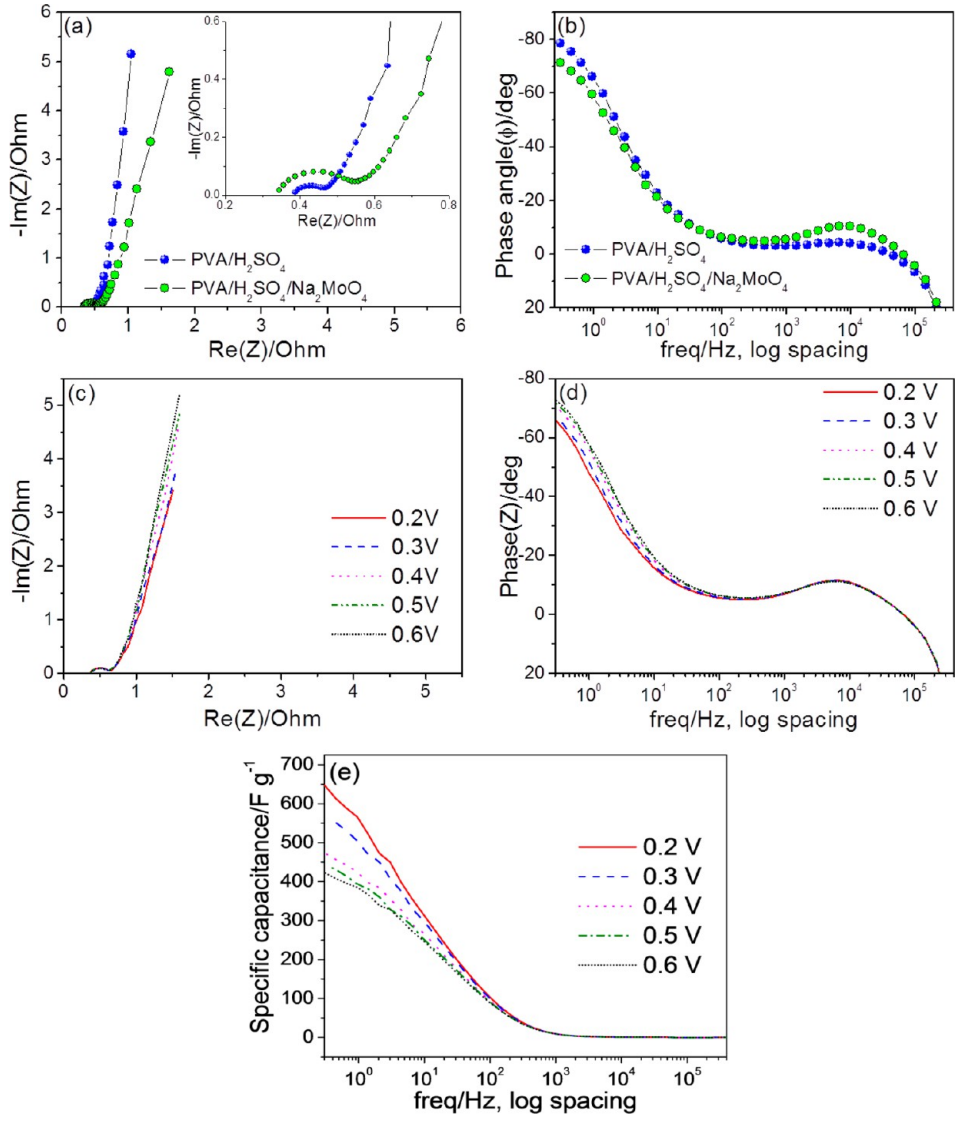

Figure 10. (a) Nyquist plots of PVA/H_2SO_4 and PVA/H_2SO_4/Na_2MoO_4. (b) Phase angle as a function of frequency of PVA/H_2SO_4 and PVA/H_2SO_4/Na_2MoO_4. (c) Nyquist plots of PVA/H_2SO_4/Na_2MoO_4 with different applied potentials (0.2−0.6 V). (d) Phase angle as a function of frequency of PVA/H_2SO_4/Na_2MoO_4 with different applied potentials (0.2−0.6 V). (e) Specific capacitance as a function of frequency of PVA/H_2SO_4/Na_2MoO_4 with different applied potentials (0.2−0.6 V).

into the PVA/H_2SO_4 gel electrolyte. Consequently, both SSEDLCs exhibit the small ~45° inclined line at middle frequency which is known as diffusive or Warburg resistance of ions with electrode.[48] Moreover, the straight line presented in the low frequency side along the imaginary axis but deviated line observed for PVA/H_2SO_4/Na_2MoO_4 gel electrolyte indicate the presence of pseudocapacitance behavior.[40,49] It is further verified using phase angle value from Figure 10b.

As expected, the lower phase angle of −70.8° was obtained for PVA/H_2SO_4/Na_2MoO_4 gel electrolyte than that for PVA/H_2SO_4 gel electrolyte (−79°). This decreased phase angle value from −79° to −70.8° specifies the change of capacitance behavior to pseudocapacitance behavior.[40] The solution resistance (R_s) and charge transfer resistance (R_{ct}) were calculated from Nyquist plot (Figure 10a). The calculated solution and charge transfer resistance are 0.38 and 0.33 Ω; 0.09 and 0.22 Ω, respectively. Here the solution resistance decreased after addition of Na_2MoO_4 into the PVA/H_2SO_4 gel electrolyte and vice versa for the charge transfer resistance. Moreover, the capacitor response frequency (f_0) at the phase angle of −45° is also shifted from 2.8 to 2 Hz (or 360 to 500 ms), so the capacitor response time is slower for PVA/H_2SO_4/Na_2MoO_4 gel electrolyte (500 ms) than for PVA/H_2SO_4 gel electrolyte (300 ms) because of their redox process. In the Nyquist plot (Figure 10c), the length of the line rapidly increased along the imaginary axis with applied potentials (from 0.2 to 0.6 V), and these kinds of changes are ascribed to the ionic diffusion into the bulk electrode as well as capacitive nature.[50] Subsequently, the phase angle (Figure 10d) also varied from −66° to −72.9°. The result of these changes with applied potential is further substantiated by the presence of pseudocapacitance nature in PVA/H_2SO_4/Na_2MoO_4 gel electrolyte used SSSC.[51] In addition, the specific capacitance also varied with applied potentials such as 646, 556, 487, 453, and 420 F g^{-1} at 0.2, 0.3, 0.4, 0.5, and 0.6 V, respectively. Hence, the better capacitance performance was obtained at the potential of 0.2 V.

The cycle life test is important for practical applications. The cycle life test was carried out for both SSEDLCs at a current density of 7.3 A g^{-1} for 3000 cycles, and results are shown in Figure 11a. The PVA/H_2SO_4 gel electrolyte used SSEDLC shows 98% of initial specific capacitance after 3000 cycles. But PVA/H_2SO_4/Na_2MoO_4 gel electrolyte used supercapacitors showed nearly ~7% decrease in specific capacitance. However, after 3000 cycles, it maintains a constant specific capacitance with capacitance retention of 93%, and this result is better than that for PVA/hydroquinone/H_2SO_4 gel electrolyte SSEDLC.[40] Moreover, the function of PVA/H_2SO_4/Na_2MoO_4 gel electrolyte used SSSC was demonstrated for practical prospects by five serially connected SSEDLCs (Figure 11b). Successfully, these five SSEDLCs turn on the 3 V blue and red light emitting diodes (LEDs) as shown in Figure 11c and d.

4. CONCLUSIONS

Activated carbon has been prepared from bio-waste of tamarind fruit shell by KOH activation. This bio-waste derived activated carbon used SSEDLC delivered the specific capacitance and energy density of 412 F g^{-1} and 9.16Wh kg^{-1}, respectively, at 1.56 A g^{-1} for PVA/H_2SO_4 gel electrolyte. Surprisingly, 57.2% of specific cell capacitance and energy density was increased after introduction of Na_2MoO_4 into the PVA/H_2SO_4 gel electrolyte, that is, 648 F g^{-1} and 14.4 Wh kg^{-1}, respectively. In addition, this device shows excellent cycle stability over 3000 cycles. These results specify that the redox pair of Mo(VI)/Mo(V) and Mo(VI)/Mo(IV) in PVA/H_2SO_4 gel electrolyte appreciably enhances both the capacitance and energy performance. Moreover, the present results propose that the tamarind fruit shell derived activated carbon and Na_2MoO_4 added PVA/H_2SO_4 gel electrolyte have promise for devising high performance SSEDLCs.

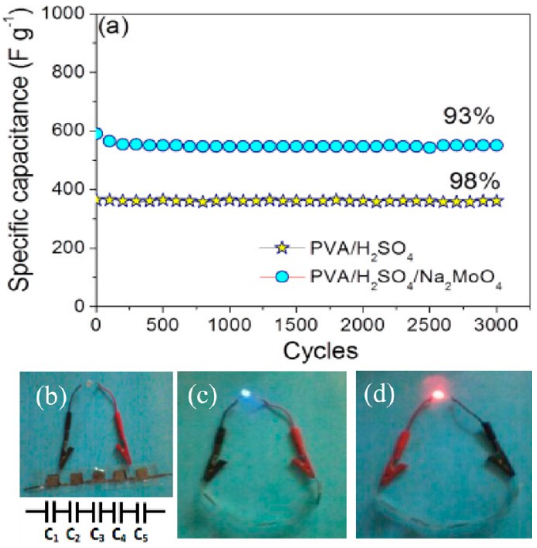

Figure 11. (a) Specific capacitance as a function of cycles at 7.3 A g^{-1}. (b) Photo of five serial SSEDLCs and LED connected with wire. (c) Blue and (d) red LEDs were powered by five charged serial SSEDLCs (see video).

■ ASSOCIATED CONTENT

Supporting Information

Additional figures and table as described in the text. This material is available free of charge via the Internet at http://pubs.acs.org.

■ AUTHOR INFORMATION

Corresponding Author

*E-mail: selvankram@buc.edu.in. Tel: +91 422 2428446. Fax: +91 422 2425706.

Notes

The authors declare no competing financial interest.

■ ACKNOWLEDGMENTS

The authors are grateful to the Department of Atomic Energy-Board of Research in Nuclear Sciences (DAE−BRNS), Government of India (No. 2010/37P/46/BRNS/1443) for their financial support.

■ REFERENCES

(1) Chen, W.; Rakhi, R. B.; Hu, L.; Xie, X.; Cui, Y.; Alshareef, H. N. *Nano Lett.* **2011**, *11*, 5165−5172.
(2) Simon, P.; Gogotsi, Y. *Nat. Mater.* **2008**, *7*, 845−854.
(3) Choudhury, N. A.; Sampath, S.; Shukla, A. K. *Energy Environ. Sci.* **2009**, *2*, 55−67.
(4) Hu, S.; Rajamani, R.; Yu, X. *Appl. Phys. Lett.* **2012**, *100*, 104413−104416.
(5) Zhou, X.; Zhou, J.; Yin, Y.; Mansour, A. N. *ECS Trans.* **2009**, *19*, 9−22.
(6) SenthilKumar, S. T.; Selvan, R. K.; Lee, Y. S.; Melo, J. S. *J. Mater. Chem. A* **2013**, *1*, 1086−1095.
(7) Wei, L.; Yushin, G. *Nano Energy* **2012**, *1*, 552−565.
(8) Biswal, M.; Banerjee, A.; Deo, M.; Ogale, S. *Energy Environ. Sci.* **2013**, *6*, 1249−1259.

(9) Wang, R.; Wang, P.; Yan, X.; Lang, J.; Peng, C.; Xue, Q. *ACS Appl. Mater. Interfaces* **2012**, *4*, 5800−5806.
(10) Mi, J.; Wang, X. R.; Fan, R. J.; Qu, W. H.; Li, W. C. *Energy Fuels* **2012**, *26*, 5321−5329.
(11) Balathanigaimani, M. S.; Shim, W. G.; Lee, M. J.; Kim, C.; Lee, J. W.; Moon, H. *Electrochem. Comm.* **2008**, *10*, 868−871.
(12) Sivasankar, V.; Rajkumar, S.; Murugan, S.; Darchen. *J. Hazard. Mater.* **2012**, *225*, 164−172.
(13) Yu, H.; Wu, J.; Lin, J.; Fan, L.; Huang, M.; Lin, Y.; Li, Y.; Yu, F.; Qiu, Z. *ChemPhyChem* **2013**, *14*, 394−399.
(14) Jun, Y. H.; Huai, W. J.; Qing, F. L.; Zhen, L. Y.; Hong, C. S.; Yuan, C.; Li, W. J.; Liang, H. M.; Ming, L. J.; Zhang, L.; Fang, H. Y. *Sci. China: Chem.* **2012**, *55*, 1319−1324.
(15) Roldan, S.; Gonzalez, Z.; Blanco, C.; Granda, M.; Menendez, R.; Santamaria, R. *Electrochim. Acta* **2011**, *56*, 3401−3405.
(16) Roldan, S.; Granda, M.; Menendez, R.; Santamaría, R.; Blanco, C. *J. Phys. Chem. C* **2011**, *115*, 17606−17611.
(17) SenthilKumar, S. T.; Selvan, R. K.; Ponpandian, N.; Melo, J. S.; Lee, Y. S. *J. Mater. Chem. A* **2013**, *1*, 7913−7919.
(18) Moutarlier, V.; Gigandet, M. P.; Pagetti, J.; Ricq, L. *Surf. Coat. Technol.* **2003**, *173*, 87−95.
(19) Li, W. S.; Tian, L. P.; Huang, Q. M.; Li, H.; Chen, H. Y.; Lian, X. P. *J. Power Sources* **2002**, *104*, 281−288.
(20) Lu, J.; Du, J. H.; Li, W. S.; Fu, J. M. *Chin. Chem. Lett.* **2004**, *15*, 703−706.
(21) Ng, K. C.; Zhang, S.; Peng, C.; Chen, G. Z. *J. Electrochem. Soc.* **2009**, *156*, A846−A853.
(22) El-Kady, M. F.; Strong, V.; Dubin, S.; Kaner, R. B. *Science* **2012**, *335*, 1326−1330.
(23) Sawangphruk, M.; Srimuk, P.; Chiochan, P.; Krittayavathananon, A.; Luanwuthi, S.; Limtrakul, J. *Carbon* **2013**, *60*, 109−116.
(24) Zhang, J.; Jiang, J.; Li, H.; Zhao, X.S. *Energy Environ. Sci.* **2011**, *4*, 4009−4015.
(25) Prasad, K. P. S.; Dhawale, D. S.; Sivakumar, T.; Aldeyab, S. S.; Zaidi, J. S. M.; Ariga, K.; Vinu, A. *Sci. Technol. Adv. Mater.* **2011**, *12*, 044602−044609.
(26) Huang, W.; Zhang, H.; Huang, Y.; Wang, W.; Wei, S. *Carbon* **2011**, *49*, 838−843.
(27) Subramanian, V.; Luo, C.; Stephan, A. M.; Nahm, K. S.; Thomas, S.; Wei, B. *J. Phys. Chem. C* **2007**, *111*, 7527−7531.
(28) Lv, Y.; Gan, L.; Liu, M.; Xiong, W.; Xu, Z.; Zhu, D.; Wright, D. S. *J. Power Sources* **2012**, *209*, 152−157.
(29) Senthilkumar, S. T.; Kumar, B. S.; Balaji, S.; Sanjeeviraja, C.; Selvan, R. K. *Mater. Res. Bull.* **2011**, *46*, 413−419.
(30) Janes, A.; Kurig, H.; Lust, E. *Carbon* **2007**, *45*, 1226−1233.
(31) Castilla, C. M.; Ramon, M. V. L; Marin, F. C. *Carbon* **2000**, *38*, 1995−2001.
(32) Rao, M. M.; Ramesh, A.; Rao, G. P. C.; Seshaiah, K. *J. Hazard. Mater.* **2006**, *B129*, 123−129.
(33) Puziy, A. M.; Poddubnaya, O. I.; Alonso, A. M.; Garcia, F. S.; Tascon, J. M. D. *Carbon* **2003**, *41*, 1181−1191.
(34) Puziy, A. M.; Podubnaya, O. I.; Socha, R. P.; Gurgul, J.; Wisniewski, M. *Carbon* **2008**, *46*, 2113−2123.
(35) Hsieh, C. T.; Teng, H. *Carbon* **2002**, *40*, 667−674.
(36) Valdes, H.; Polo, M. S.; Utrilla, J. R.; Zaror, C. A. *Langmuir* **2002**, *18*, 2111−2116.
(37) Frackowiak, E. *J. Braz. Chem. Soc.* **2006**, *6*, 1074−1082.
(38) Su, D. S.; Schogl, R. *ChemSusChem* **2010**, *3*, 136−168.
(39) Taberna, P. L.; Simon, P.; Fauvarque, J. F. *J. Electrochem. Soc.* **2003**, *150*, A292−A300.
(40) Senthilkumar, S. T.; Selvan, R. K.; Ponpandian, N.; Melo, J. S. *RSC Adv.* **2012**, *2*, 8937−8940.
(41) Nakayama, M.; Tanaka, A.; Sato, Y.; Tonosaki, T.; Ogura, K. *Langmuir* **2005**, *21*, 5905−5913.
(42) Suppes, G. M.; Cameron, C. G.; Freund, M. S. *J. Electrochem. Soc.* **2010**, *157*, A1030−A1034.
(43) Panday, G. P.; Rastogi, A. C. *J. Electrochem. Soc.* **2012**, *159*, A1664−A1671.
(44) Yuan, L.; Lu, X. H.; Xiao, X.; Zhai, T.; Dai, J.; Zhang, F.; Hu, B.; Wang, X.; Gong, L.; Chen, J.; Hu, C.; Tong, X.; Zhaou, J.; Wang, Z. L. *ACS Nano* **2012**, *6*, 656−661.
(45) Rathod, D.; Vijay, M.; Islam, N.; Kannan, R.; Kharal, U.; Kurungot, S.; Pillai, V. *J. Appl. Electrochem.* **2009**, *39*, 1097−1103.
(46) Hashmi, S. A.; Latham, R. J.; Linford, R. G.; Schlindwein, W. S. *Polym. Int.* **1998**, *47*, 28−33.
(47) Xia, X.; Tu, J.; Mai, Y.; Chen, R.; Wang, X.; Gu, C.; Zhao, X. *Chem.—Eur. J.* **2011**, *17*, 10898−10905.
(48) Zheng, H.; Zhai, T.; Yu, M.; Xie, S.; Liang, C.; Zhao, W.; Zhang, Z.; Lu, X. *J. Mater. Chem. C* **2013**, *1*, 225−229.
(49) Yu, H.; Fan, L.; Wu, J.; Lin, Y.; Huang, M.; Lin, J.; Lan, Z. *RSC Adv.* **2012**, *2*, 6736−6740.
(50) Niu, Z.; Dong, H.; Zhu, B.; Li, J.; Hng, H. H.; Zhou, W.; Chen, X.; Xie, S. *Adv. Mater.* **2013**, *25*, 1058−1064.
(51) Sugimoto, W.; Iwata, H.; Yokoshima, K.; Murakami, Y.; Takasu, Y. *J. Phys. Chem. B* **2005**, *109*, 7330−7338.